# Estimating bird flight height using 3-D photogrammetry

Prinsloo ND[1]*, Postma M[1*], Ryan PG[2], Coetzee M[1] & De Bruyn PJN[1]

[1] Mammal Research Institute, Department of Zoology and Entomology, University of Pretoria, Private Bag X20, Hatfield 0028, South Africa.

[2] FitzPatrick Institute of African Ornithology, DSI-NRF Centre of Excellence, University of Cape Town, Rondebosch 7701, South Africa.

*Corresponding author: nicolas.prinsloo7@gmail.com

Running page heading: stereophotogrammetric bird flight height

**Abstract**

Harnessing wind or solar power have become popular “green” options for energy production. However, colliding with wind turbine blades or being burned by concentrated solar flux around power towers can present a substantial threat to birds. Assessing the severity of this risk to different bird species requires accurate estimates of their flight height. We developed a three-dimensional (3-D) stereophotogrammetric approach to determine bird flight heights. The accuracy of four varying stereophotogrammetric camera layouts were compared between each other and against laser-based rangefinder measurements of static structures. Bird flight heights were measured and compared between species and repetitive photographic captures over short time periods were tested for autocorrelation. Three out of four camera layouts performed equally well when measuring static structures at distances of up to 100 m (0.0 ± 0.3%; or 0.00 ± 0.03 m error), better than laser-based rangefinders (0.3 ± 4.8%; or 0.12 ± 0.51 m error) on a small target. Photogrammetrically measured flight heights were precise to 0.07 ± 0.05 m up to ~275 m away and to within 1 m at 400 m, and measurable up to ~535 m away. Using this tested approach, repetitive, sequential flight heights of moving birds were significantly autocorrelated compared to random flight heights ($p$ = 0.001). Species-specific flight heights were distinct, practically demonstrating the approach’s potential application, however, scarcity of flight height data prompts further application of the approach to record distributions of flight height. This stereophotogrammetric method was accurate, cost-effective, objective, and relatively simple to apply. It could measure flight heights, and potentially micro-avoidance behaviour in 3-D flight patterns, to ultimately identify species that are at potential risk of collision or burning with wind turbines and solar towers.

**Key-words:** bird flight height, renewable energy, photogrammetry, turbine collision, wind farm, CSP tower

## Introduction

The ecological impact of wind farms and various solar power generation technologies are thought to be benign compared to fossil fuels; contributing little to atmospheric emissions and waste (Saidur *et al.*, 2011; Leung & Yang, 2012; Khan & Arsalan, 2016). However, wind farms and large-scale solar power facilities can negatively impact wildlife populations through habitat modification (Masden *et al.*, 2010; Jeal *et al.*, 2019b, 2019a; Visser *et al.*, 2019). Animals that fly through wind farm turbine rotor sweep areas run the risk of collision or barotrauma, resulting in injury or death (Everaert & Stienen, 2006; Thaxter *et al.*, 2017), and those flying through the 'solar flux' airspace of utility-scale solar energy (USSE) towers can be injured or killed by the heat (Diehl *et al.*, 2016; Walston *et al.*, 2016). Such additive mortality rates can severely impact populations of long-lived, slow reproducing animals (Barrios & Rodríguez, 2004; Everaert & Stienen, 2006). Collision depends on certain morphological characteristics and flight behaviour to increase the frequency of birds co-occurring with turbine blades (Thaxter *et al.*, 2017). Flight speed (Stantial & Cohen, 2015), agility (de Lucas *et al.*, 2008), micro- and macro-avoidance rates (Cook *et al.*, 2012; Everaert, 2014) all influence collision risk.

To assess collision risk, accurate estimates of flight heights are required (Stantial & Cohen, 2015; Harwood, Perrow & Berridge, 2018). Collision risk predictive models could be misrepresented without flight height data or compounded by inaccurate measurements, especially for rarer species (Stewart, Pullin & Coles, 2007; Ferrer *et al.*, 2012). Unfortunately, flight height data are often insufficient in quantity and quality, and many studies simply default to estimates by surveyors (Band, 2012; Harwood *et al.*, 2018). Surveyors can be trained to estimate flight heights relative to fixed structures, and then allocate bird heights to flight bands (e.g. Osborn & Dieter, 2009; Stantial & Cohen, 2015; Harwood *et al.*, 2018). However, this method is subjective and prone to underestimation, especially with fatigued observers and when measurements are taken before infrastructure construction when no comparative heights are available in the field of reference (Stantial & Cohen, 2015; Harwood *et al.*, 2018). Optical laser rangefinders are accurate for single large birds up to 100 m away and 50 m high but yield inaccurate results or fail to yield any measures at all for multiple small, distant, irregular, and fast-flying birds (Desholm *et al.*, 2006; Stantial & Cohen, 2015; Wulff *et al.*, 2016; Borkenhagen, Corman & Garthe, 2018; Harwood *et al.*, 2018). The use of fixed-beam radars and thermal imaging is limited in spatial manoeuvrability (Gauthreaux & Livingston, 2006) and radar systems are expensive (*ca* US$60 000), large and cumbersome to use (Desholm *et al.*, 2006; Diehl *et al.*, 2016). Currently, the most accurate systems are LiDAR, which estimate heights to within 1 m for birds up to 150 m away from the sensor (Cook *et al.*, 2018), and radar, in a 1.5 km radius (Krijgsveld *et al.*, 2009; Strumpf *et al.*, 2011). To capture flight heights of all birds passing through a wind farm at least once, two perpendicular radar systems are vertically tilted with one radar plane perpendicular to the direction most travelled, doubling the expense and complexity (Krijgsveld *et al.*, 2009; Strumpf *et al.*, 2011). Furthermore, without additional photographs or observers, radar might not be specific enough to assign records to species (Péron *et al.*, 2020). GPS-loggers and/or altimeters are effective in collecting continuous long-term flight height data, but are restricted to larger birds, are often short-lived, require invasive capture and recapture of birds, which is costly, limits sample sizes and may affect bird behaviour (Corman & Garthe, 2014; Garthe *et al.*, 2014; Cleasby *et al.*, 2015; Borkenhagen *et al.*, 2018). Furthermore, the accuracy of resulting data may be compounded if it is incorrectly handled (Corman & Garthe, 2014; Péron *et al.*, 2017, 2020). These methods vary greatly in cost, ease of use, accuracy and repeatability.

These challenges emphasise the need for an accurate, cost-effective, practical alternative to estimate bird flight heights (Stewart *et al.*, 2007; Hill & Arnold, 2012). We demonstrate the use of three-dimensional photogrammetry, “measurements from photographs”, as an alternative solution. We test various configurations of a compact and relatively inexpensive stereophotogrammetric approach (*ca* US$2 000), which can repeatedly capture concurrent overlapping images to measure flight height above a ground plane in the field of view. Unlike the spatially calibrated (for specific camera positions and orientations) stereo-videography used by Wu *et al.*, (2009) and Theriault *et al.*, (2010), we only calibrate for intrinsic camera parameters (i.e. lens distortion) before an easy field set-up to objectively determine flight heights above a ground plane. We assessed the precision and accuracy of height estimates of known items compared to laser-based measurements, then applied the approach through repeated flight height measurements for a range of bird species with varied sizes and flight speeds.

**Materials and Methods**

The stereophotogrammetric approach was tested and applied at the LC de Villiers sports ground of the University of Pretoria (25.7510° S, 28.2481° E). Three calibrated (see calibration details in Postma, Bester & de Bruyn, 2013) Canon 1300D DSLR cameras with 18–55 mm Canon lenses were placed on tripods in four configurations (two linear and two angled; Fig. 1). These were used to photogrammetrically measure known dimensions of a rugby post 50–100 m (at 10 m distance intervals) from the central camera for comparison against laser-based rangefinder measurements. A 2-m scale measure was placed near the object of interest. The cameras were manually focused and wirelessly connected to a single remote trigger (YONGNUO RF603C II, Yong Nuo Ltd., Hong Kong) to ensure simultaneous shutter release. Settings for f-stop (*f*/22), shutter speed (1/1600s), ISO value (ISO 6400), and focal length (55

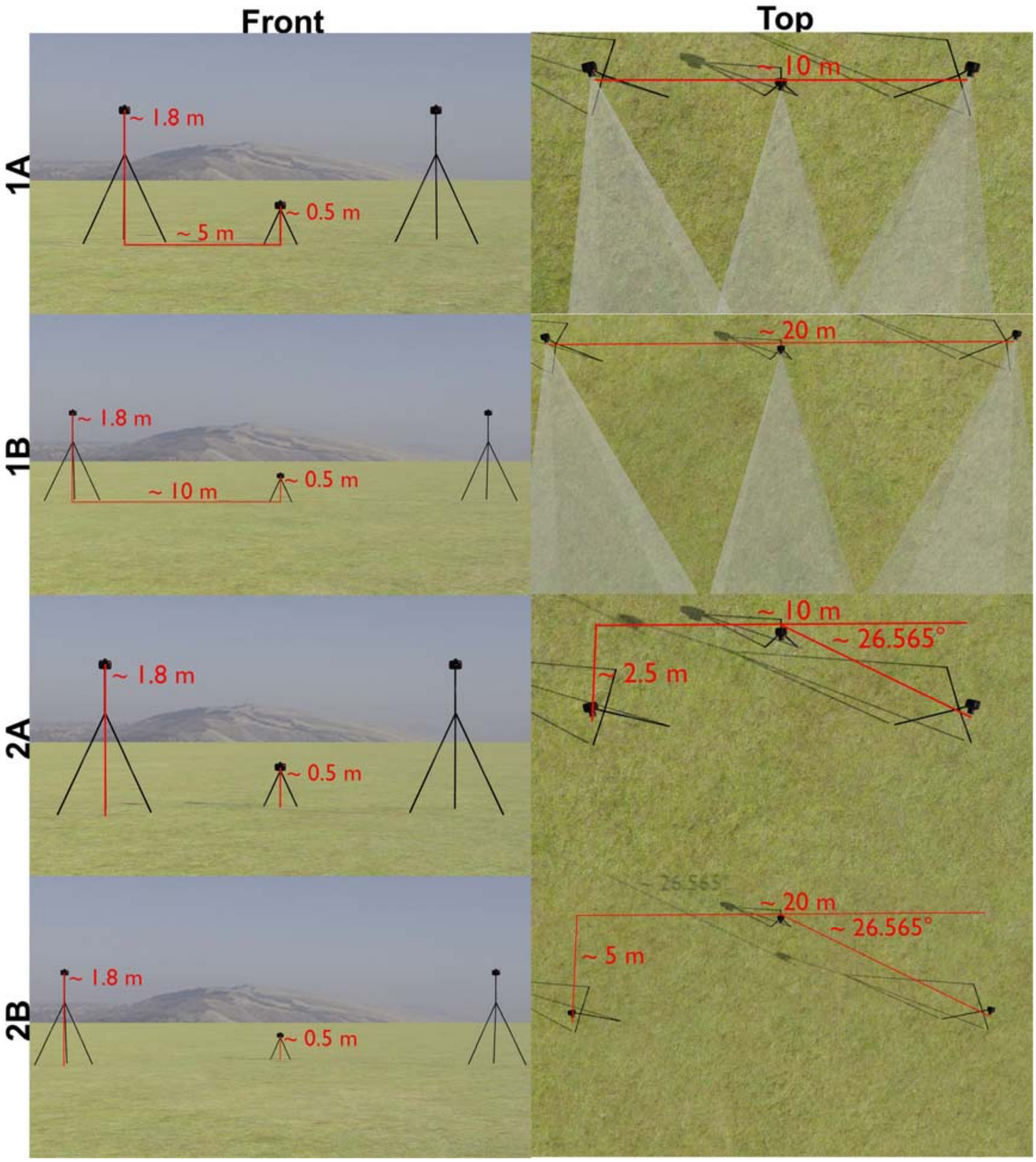


**Figure 1**. Four camera configurations (1A, 1B, 2A & 2B) used to photograph a known sized object (static test) at 10 m intervals from 50–100 m. Three cameras on tripods were placed 10 m (1A & 2A) or 20 m (1B & 2B) apart. Cameras of configurations (1A & B) were placed linearly, while cameras of configurations (2A & B) were placed ~ 26.565° (~2.5 or 5 m, respectively) forward from the central camera. Cameras were at different heights off the ground. Textures and high dynamic range images are from Poliigon (www.poliigon.com). Configurations were modelled within Blender (Blender Online Community, 2019).

mm) were standardised for all cameras to take JPG images (5184 × 3456 pixels). We measured the distances between the central points on camera lenses with a tape measure. Two additional structures, a floodlight on a rugby field and a structure alongside a dam, were included in the study. The angle of intersection was the angle between intersecting rays from the centres of the lenses to a single point at the base of the structure. To maintain an angle of intersection ($a_i$) > 5° for more distant structures (200.8 to 228.2 m away), we used an angled configuration with each camera 20 m apart ($a_i$: 5.22° to 5.96°), instead of 5 m ($a_i$: 1.27° to 1.44°) or 10 m ($a_i$: 2.56° to 2.91°) as in configurations 2A and 2B, respectively. A measurable object already present in each scene was used for scale. During tests, 317 birds of at least 13 species were photographed in flight (Table 1).

*Photogrammetry*

Photographs were imported into PhotoModeler® Scanner (EOS systems Inc., Vancouver) and used to replicate the scene in 3-D, including birds and static objects (a project). Calibrations were assigned to each camera. We used the SmartMatch® function with default settings, which automatically identified and cross-referenced unique features to triangulate the camera positions and orientations. The quality of each project was evaluated by the software's calculated root-mean-squared (RMS) precision values (pixels) between feature positions on different photos (de Bruyn *et al.*, 2009).

In the 3-D scene, we manually identified and cross-referenced two structural dimensions on a set of rugby posts. Thereafter, the project was processed to optimise landmark errors and camera orientations, and the dimensions were photogrammetrically measured. We replicated the analytical component three times for each of the three field replicates at 10-m intervals from 50 to 100 m (from the object of interest) for all four camera configurations (*n* =

**Table 1.** Sample sizes (enough for preliminary comparison*) for bird taxa or ecomorphs with independent sample size in brackets. The mean ± standard deviation was calculated for the independent samples, and the maximum flight height was recorded.

| **Bird/Ecomorph** | **Taxon** | ***n (ind.)*** | **Flight height (m)** | |
|---|---|---|---|---|
| | | | **Mean ± SD** | **Maximum** |
| Small | | 44 (42)* | 14.7 ± 9.1 | 36.6 |
| Aerial insectivores | Hirundinidae/Apodidae | 44 (36)* | 14.7 ± 9.1 | 36.6 |
| Medium | | 44 (28)* | 15.8 ± 9.0 | 37.8 |
| Reed cormorant | *Microcarbo africanus* | 7 (2) | 12.8 ± 2.0 | 14.2 |
| Doves/pigeons | Columbidae | 30 (18)* | 19.4 ± 8.0 | 37.8 |
| Feral pigeon | *Columba livia* | 18 (10) | 20.0 ± 6.7 | 29.3 |
| Laughing dove | *Spilopelia senegalis* | 2 (2) | 18.9 ± 5.2 | 20.3 |
| Red-eyed dove | *Streptopelia semitorquata* | 3 (2) | 22.8 ± 21.2 | 37.8 |
| Unidentified doves | Columbidae | 7 (5) | 13.2 ± 3.3 | 21.6 |
| Blacksmith lapwing | *Vanellus armatus* | 4 (4) | 0.6 ± 0.2 | 3.9 |
| Common myna | *Acridotheres tristis* | 2 (2) | 5.6 ± 0.5 | 6.0 |
| Karoo thrush | *Turdus smithi* | 2 (2) | 8.7 ± 0.2 | 8.6 |
| Large | | 105 (54)* | 20.5 ± 19.7 | 94.8 |
| Pied crow | *Corvus albus* | 7 (2) | 33.7 ± 7.0 | 48.7 |
| Western cattle egret | *Bubulcus ibis* | 24 (19)* | 4.8 ± 3.2 | 9.9 |
| Egyptian goose | *Alopochen aegyptiacus* | 4 (2) | 0.4 ± 0.3 | 1.1 |
| Black-headed heron | *Ardea melanocephala* | 9 (5) | 20.0 ± 19.9 | 56.9 |
| Sacred ibis | *Threskiornis aethiopicus* | 61 (26)* | 26.0 ± 20.4 | 94.8 |
| Unidentified birds | | 123 (98) | 23.2 ± 14.0 | 75.1 |
| **All species** | | 316 (222) | 19.4 ± 15.8 | 94.8 |

72) and calculated a percentage measurement error. Two additional structures (building and floodlight) were used as sufficiently tall proxies for wind turbines or solar towers at varying distances from the cameras for comparison with rangefinder measurements. Additionally, we constructed a dense surface model (DSM) to illustrate the 3-D scene in PhotoModeler® Scanner. Automatic and manual steps were timed ($n$ = 10).

To briefly illustrate the practical applicability, bird flight height was taken as the vertical distance between the bird's central 3-D position and a best-fit plane, created between four ground features (Fig. 2). We identified birds as far as taxonomically possible, but due to inconsistent difficulty in visually distinguishing between martins, swifts, and swallows with pixilation at great distances, we decided to lump them together under aerial insectivores.

*Statistical Analysis*

A significance threshold ($p < \alpha$) was set at 0.05 with marginality at 0.1. Means were reported ± standard error (SE), to illustrate repeatability of the mean alongside percentage error after mean centering. R, version 3.5.1 (R Development Core Team, 2018), was used for statistical analyses. Percentage error (%) was non-normal, so a Kruskal-Wallis and a multiple comparison post hoc test were used to assess accuracy between the four different configurations between 50 and 100 m away. Error was interpolated over distance using a loess smoothing function.

Parametric linear regression assumptions were tested using the Global Validation of Linear Model Assumptions (*gvlma*) package (Peña & Slate, 2006). For estimates of structural dimensions, we applied four smoothing iterations in the *KernSmooth* package to non-parametrically illustrate the general trend in overall RMS errors with the angle of intersection (Wand, 2013). Structural heights by photogrammetry and rangefinder were compared using a

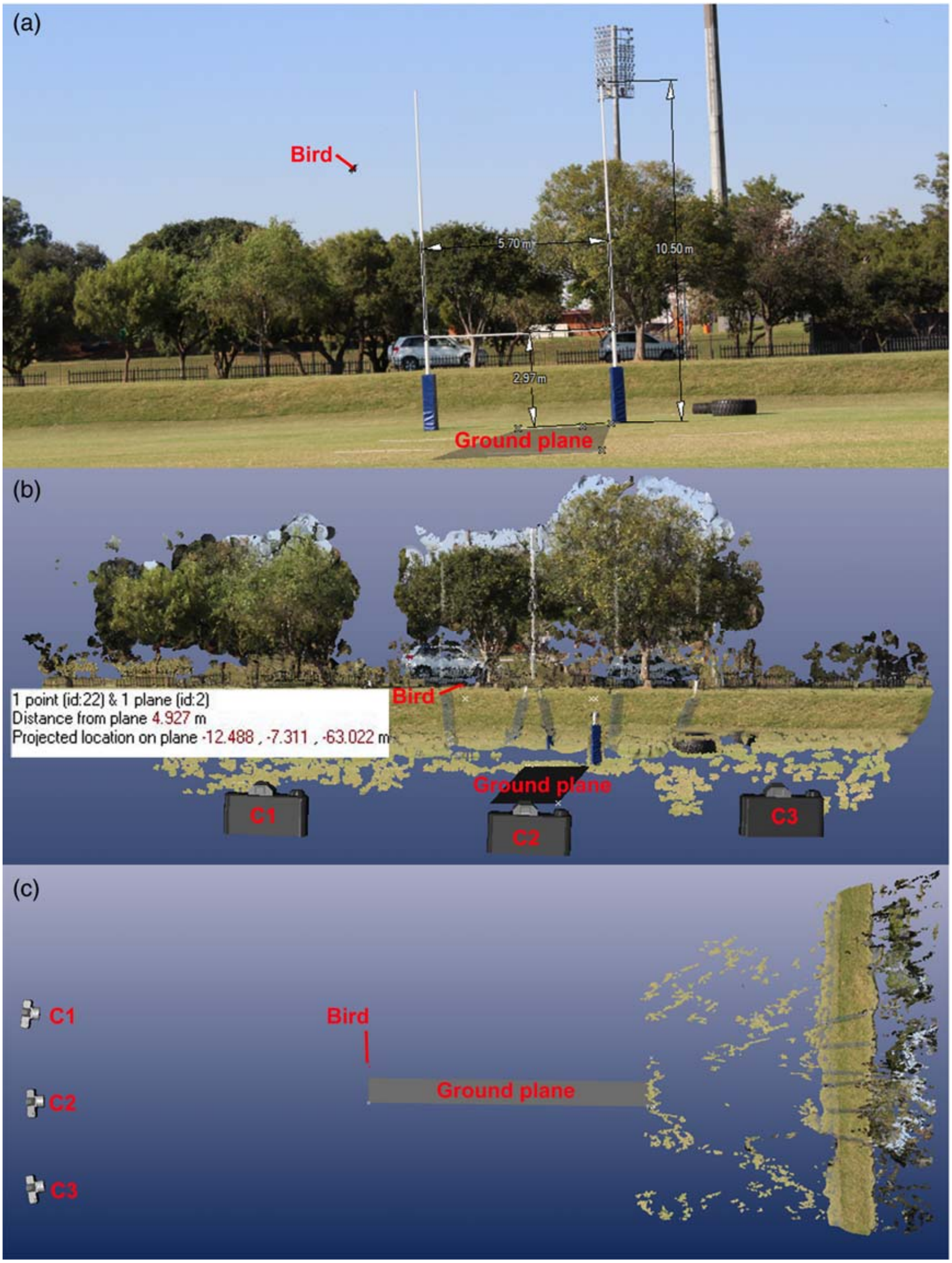


**Figure 2**. An example of the configuration 2B used to create a 3-D scene from photos. (a) Central photo. (b) Front view from behind camera positions in the 3-D scene. (c) Top view above the 3-D scene. The central cameras were 70 m from the static object (rugby posts). A line indicates the position of a swallow in flight, and its flight height is 4.93 m. The length between manually cross-referenced marks (x) on a pole on the ground provides scale to this 3-D scene.

pairwise Wilcoxon rank-sum test because the variance in replicated structural heights was not homogenous across structures. The absolute percentage error was compared between the rangefinder and photogrammetric measurements using a Kruskal-Wallis test.

Mean flight heights and distances from the central camera were reported ± standard deviation (SD), to illustrate the average differences in flight height around the mean. The effect of distance on measurement error was tested using parametric linear regression. Measuring flight height accuracy of moving birds is difficult without synchronizing two different configurations, but for repeated photo captures over short periods, 0 to 3 s (~2 ± 2 s), we expect similar consecutive flight heights of individual birds. An autocorrelation function (ACF) quantified correlation between consecutive bird flight heights ordered by known individuals and site, and site only, and a randomly ordered control. The first five ACF values were compared using ANOVA. The *ggplot2* package was used to visualize results (Wickham, 2016).

We used trigonometry and known dimensions of the camera configurations to replicate their fields of view (°) in 2-D and determine the expected vertical and horizontal area covered by the overlapping fields of view (supplementary Fig. S3 & S4). We also estimated how these areas would increase with increasing distance between the cameras and the focal structures, and distance behind the focal structures (see supplementary material S2 for further details). Thereafter, we determined how the constraints imposed between these two areas of coverage might interact to affect the maximum height that could possibly be measured at varying distances from the camera.

## Results

*Structure height*

The cameras were deployed in the field and were manually triggered to capture passing birds for a net time of 1 h 23 minutes, capturing a total of 252 projects at an average rate of 3 per minute. Within photogrammetry software, automatic (SmartMatch and processing) steps took approximately 51 ± 17 s, and manual steps (cross-referencing landmarks, assigning the known scale, and measuring an unknown dimension) took 195 ± 16 s to complete a single project with a single height measurement. For all 252 projects, the manual steps took a total of 13 h 39 min ± 1 h 7 min 12 s, and the automatic steps totalled 3 h 34 min 12 s ± 1 h 11 min 24 s to complete single height measurements. For every 10 minutes of photo capture in the field, there are approximately 30 projects with 25 min 48 s ± 8 min 36 s of automatic steps and 1 h 38 min 40 s ± 8 min 6 s of manual steps. For each project, there were 1 structural height and 1.25 bird flight height measurements; additional heights did not proportionally increase time on the manual steps as a scale and the ground planes were already specified.

Percentage measurement errors were significantly greater ($\chi^2_3$ = 81.35; $p$ < 0.001) in camera configuration 1A (-3.31 ± 0.36%) than the other three camera configurations (0.00 ± 0.02%). Increasing the distance between adjacent cameras to 10 m in the linear setup had similar accuracy to the two angled configurations (Table 2; Fig. 3). Distance from the object of interest did not significantly affect accuracy from 50 to 100 m. The overall project quality (RMS error) was 0.6 ± 0.2 pixels with maximum residuals of 2.9 ± 1.8 pixels; considered good for large scenes, as in this case. This RMS error was minimized at an angle of intersection (*a. i.*) of ~5° (Fig. 4). There were significant differences between measured heights of the three different structures, but not between their respective photogrammetry and rangefinder measurements (Table 3). Percentage error in rangefinder measurements surpassed 5% for the

**Table 2.** A. Multiple comparison Kruskal post hoc test assessed photogrammetric measurement accuracy between the four different configurations. Observed differences are presented for Kruskal Wallis test, with ticks above a critical threshold of 18.405. B, error associated with setups, error range (% & mm) are reported with mean ± standard error (% & mm).

| **A. DIFFERENCES BETWEEN CONFIGURATIONS** | | |
|---|---|---|
| **Setup Compared** | **Observed Difference** | **Different** |
| 1A vs. 1B | 24.972 | TRUE |
| 1A vs. 2A | 27.472 | TRUE |
| 1A vs. 2B | 20.889 | TRUE |
| 1B vs. 2A | 2.500 | FALSE |
| 1B vs. 2B | 4.083 | FALSE |
| 2A vs. 2B | 6.583 | FALSE |

| **B. ERROR ASSOCIATED WITH CONFIGURATIONS** | | | | |
|---|---|---|---|---|
| **Setup ID** | **Percentage** | | **mm** | |
| | **Range** | **Mean ± SE** | **Range** | **Mean ± SE** |
| 1A | -7.85 to 5.08% | -3.31 ± 0.356% | -677 to 474 | -210 ± 27 |
| 1B | - 0.67 to 0.63% | -0.04 ± 0.002% | -41 to 65 | 4 ± 2 |
| 2A | -0.63 to 0.90% | 0.00 ± 0.002% | -43 to 27 | -1 ± 2 |
| 2B | -1.07 to 1.11% | -0.04 ± 0.002% | -38 to 35 | -2 ± 2 |

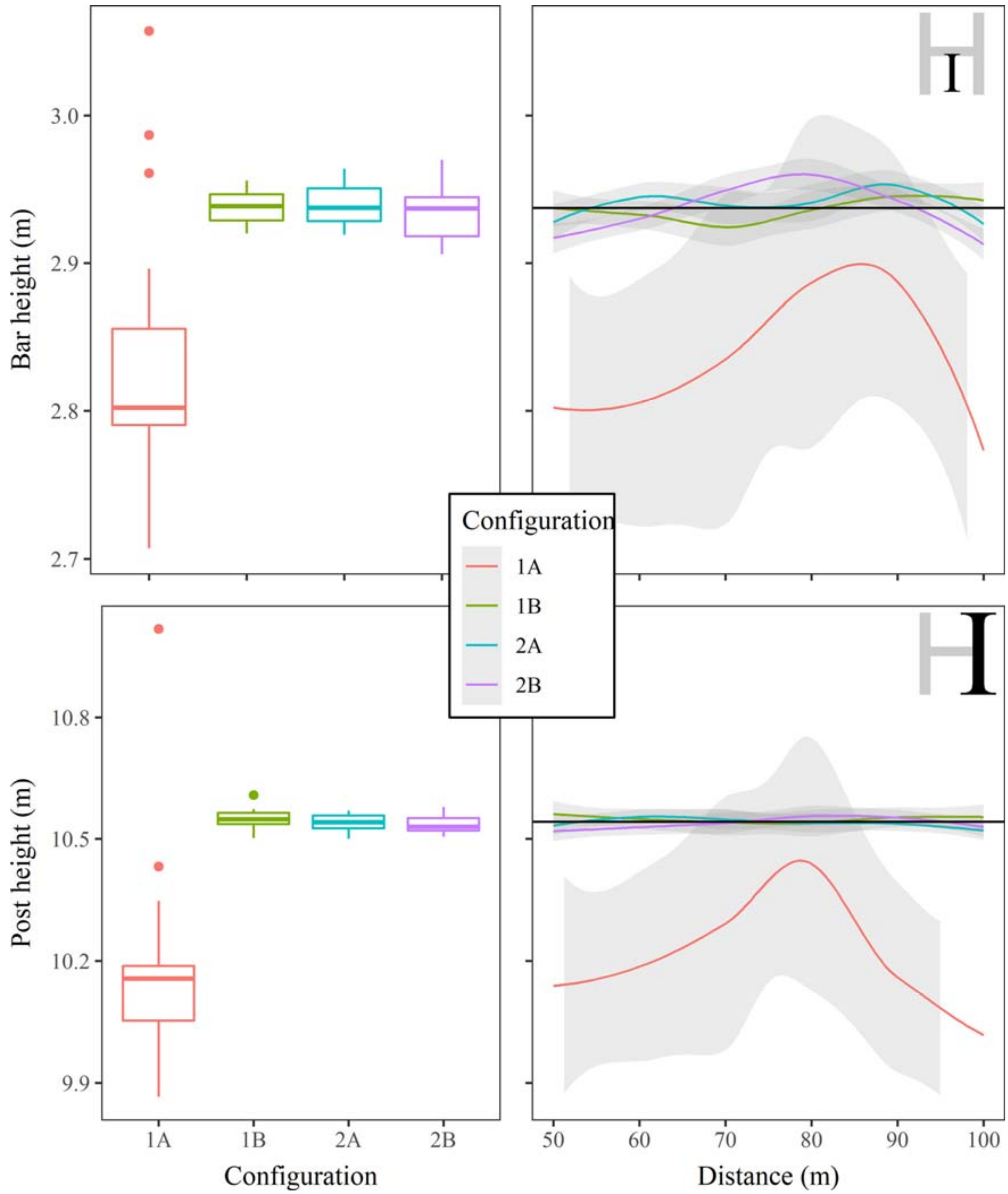


**Figure 3**. Measurements of the bar and rugby post heights (top right) in Fig. 2 estimated with four different camera configurations (1A, 1B, 2A, 2B) (first column; median, inter-quartile range, and outliers). The second column depicts measurement variation in relation to camera distance from the measured object, applying a loess smoothing function. The solid black line is the global mean of the more precise measurements (1B, 2A, and 2B).

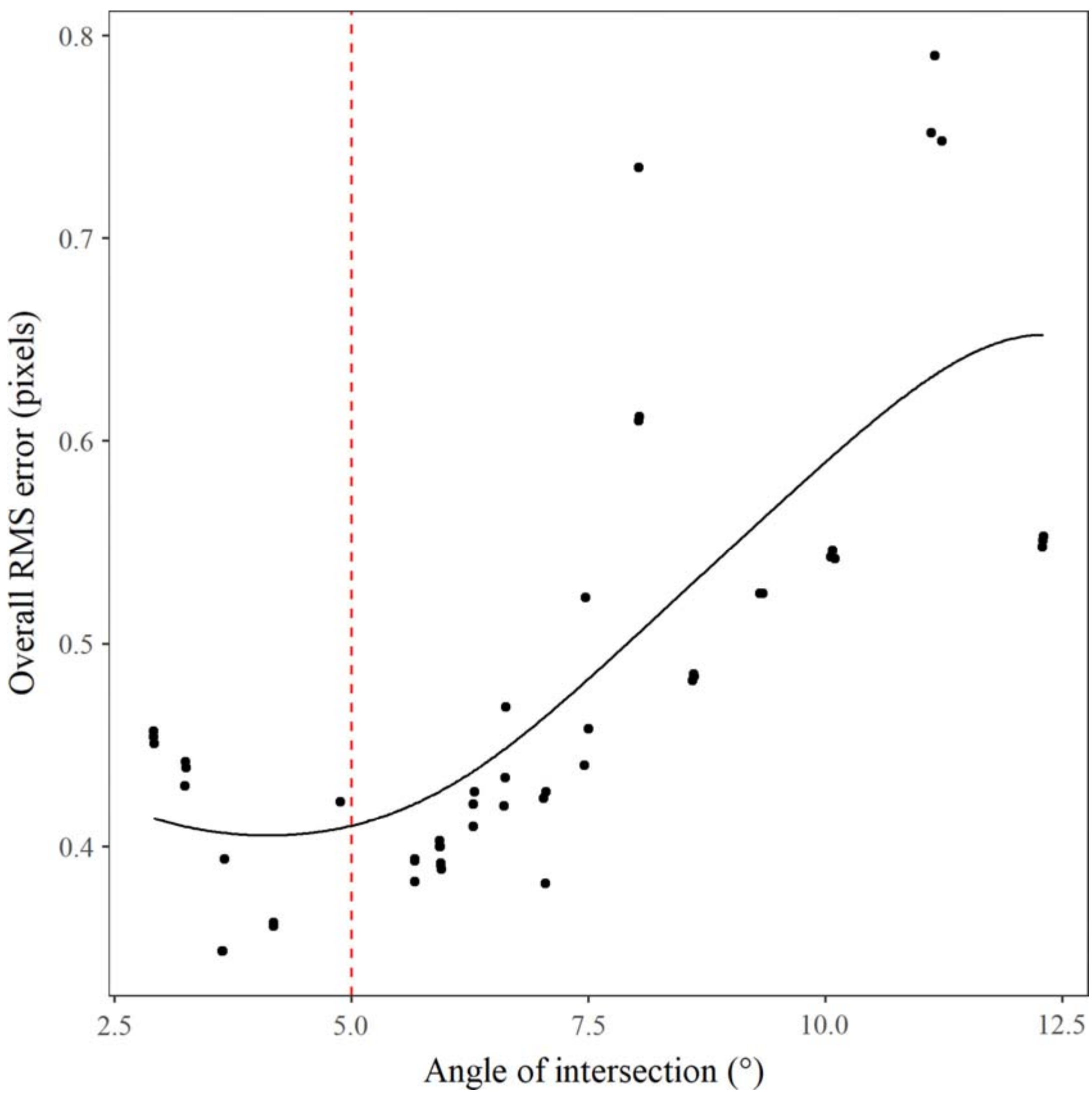


**Figure 4.** The relationship between the angle of intersection (°) and the overall root mean squared (RMS) error (pixels), a proxy of project quality.

**Table 3.** Photogrammetry and rangefinder height (m) mean ± standard error for the rugby post, floodlight, and sports building. The *p*-values resulting from a pairwise Wilcoxon rank sum test correspond to row or column differences.

| **Approach to measure structure height** | Rugby post | *n* | Building | *n* | Floodlight | *n* | ***p*-value** |
|---|---|---|---|---|---|---|---|
| Photogrammetry (m) | 10.543 ± 0.003 | 54 | 30.842 ± 0.060 | 147 | 44.577 ± 0.043 | 50 | **<0.001** |
| Rangefinder (m) | 10.56 ± 0.273 | 10 | 31.196 ± 0.064 | 10 | 44.940 ± 0.249 | 10 | **<0.003** |
| ***p*-value** | **1** | | **0.08** | | **1** | | |
| **Trait** | Rugby post | | Building | | Floodlight | | |
| Distance away (m) | 50.841 to 100.895 | | 227.77 ± 0.451 | | 200.99 ± 0.222 | | |
| Angle of intersection | 2.908° to 12.35° | | 5.24 ± 0.14° | | 5.97 ± 0.05° | | |

rugby posts (Fig. 5) and was significantly higher than in photogrammetric measurements ($\chi^2_1$ = 14.74; $p$ < 0.001).

*Bird flight height*

We photogrammetrically measured flight heights ($n$ = 316) of at least 13 bird species (Table 1). Between 38.1 m and 273.4 m away, the measurement error was 0.07 ± 0.05 m, which increased with distance ($F_{1,82}$ = 100.1; $p$ < 0.001; $R^2$ = 0.544; Fig. 6). Flight heights ranged from 0.1 m (a swallow hawking over a lawn) to 95 m above the ground (a sacred ibis, *Threskiornis aethiopicus*). Sequential flight heights of moving individual birds ($n$ = 222) were significantly more autocorrelated than the randomly ordered control dataset ($p$ < 0.001), and a dataset ordered by site ($p$ = 0.005) (Fig. 7). This suggests time-dependence in bird flight heights of individuals over short periods, supporting the accuracy of photogrammetric measurements for moving birds with minor changes in flight height. No significant differences occurred between the flight heights of large, medium, and small birds ($p$ = 0.2). Herein, egrets flew at significantly lower heights than doves ($p$ < 0.001), ibises ($p$ = 0.02) or aerial insectivores ($p$ < 0.001).

*Trigonometric Calculations*

Intuitively and based on trigonometric calculations, we expect horizontal (Fig. S6) and vertical area (Fig. S9; $m^2$) covered by the overlapping fields of view to increase with increasing distance between the central camera and the focal object of interest (e.g. rugby posts; see supplementary material for more detailed results). For camera configurations that are too close to the object of interest, 10-50 m, their necessary rotation inwards and downwards would reduce the horizontal (Fig. S5) and vertical coverage (Fig. S8), and measurable flight height (Fig. S12). The downward (or lack of upward) rotation is necessary to sufficiently intersect the substrate to

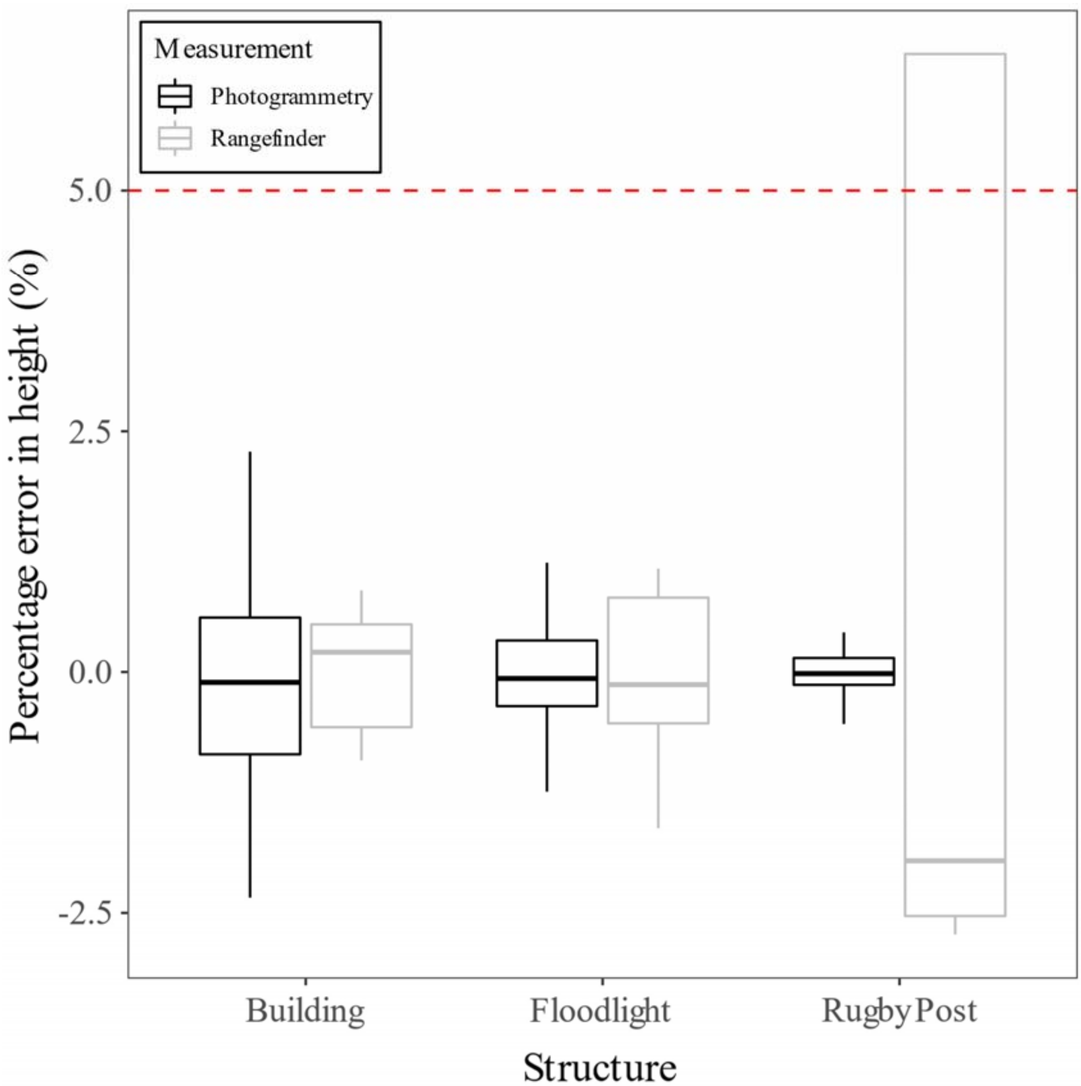


**Figure 5**. Percentage error (%) of building, floodlight, and rugby post height measurements using photogrammetry (black) and a rangefinder (grey).

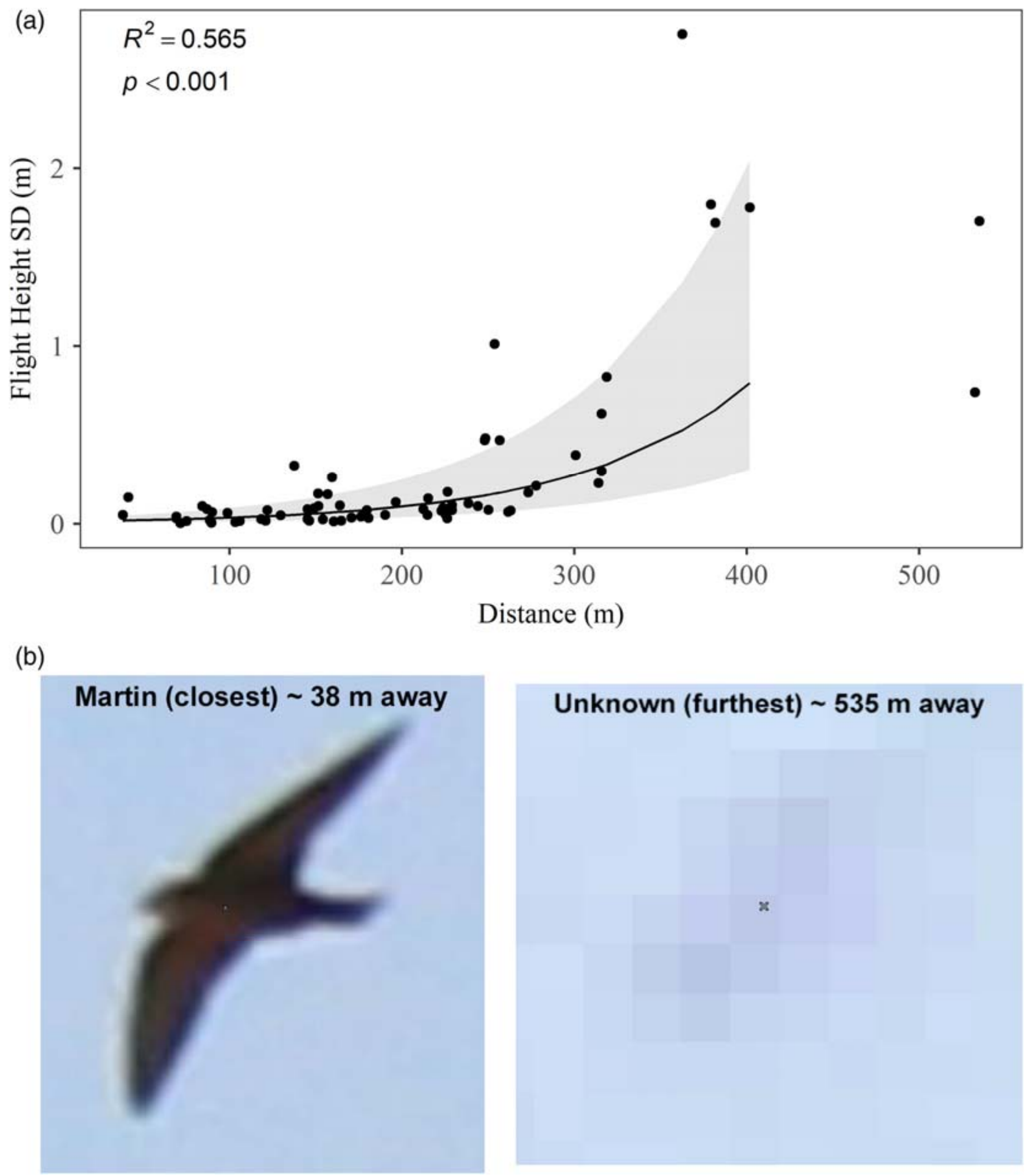


**Figure 6.** (a) The exponential increase ($F_{1,82} = 100.1$; $P < 0.001$; $R^2 = 0.544$) in bird flight height standard deviation (m) with increasing distance from the central camera (m). (b) As distance decreased, birds became less pixelated, and easier to pinpoint their centres (marked with an x).

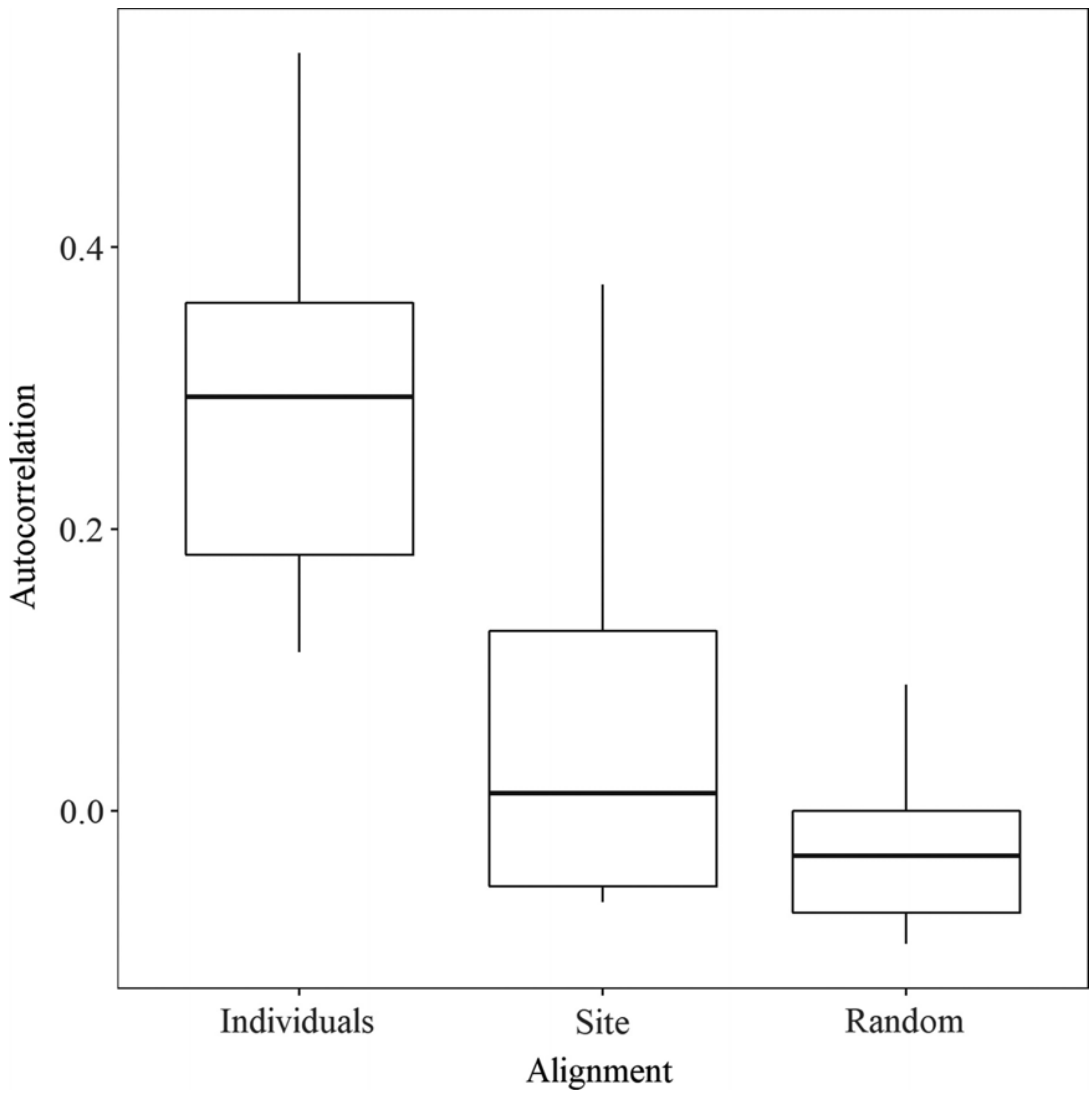


**Figure 7.** The time-dependencies, proxied by autocorrelation, of data ordered sequentially by individual (individuals), randomly within site (site), and randomly overall (random) ($F_{2,12}$ = 6.098; $P$ = 0.015).

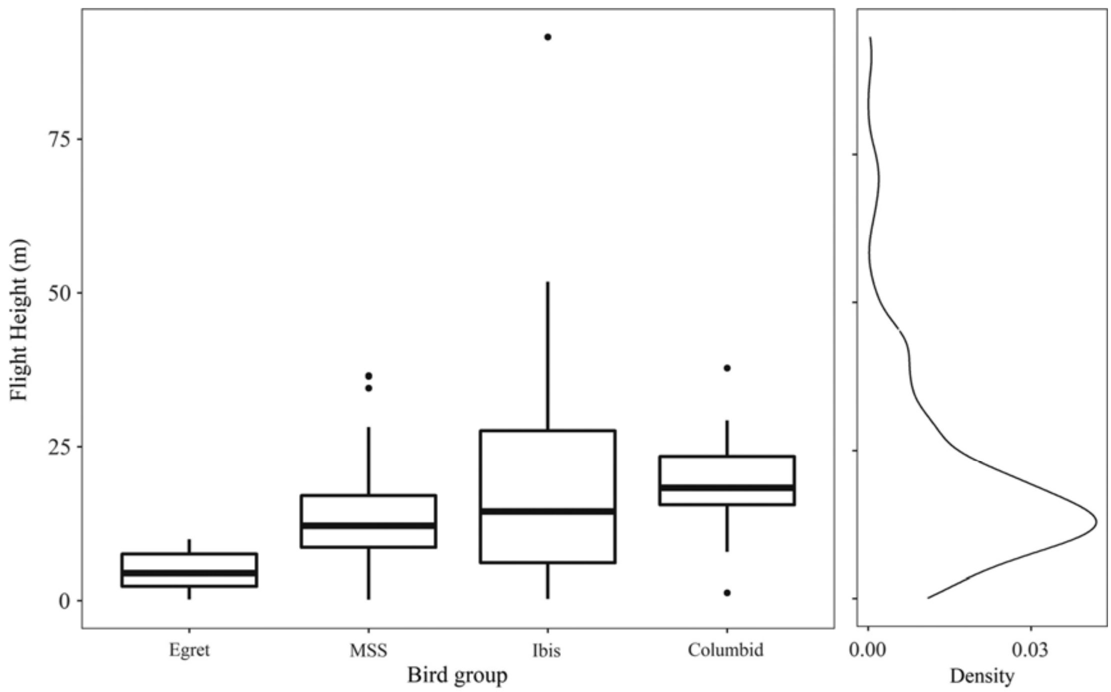


**Figure 8.** Photogrammetrically measured flight heights with time dependent data of individuals removed, for bird groups with sufficient sample size ($n \geq 10$) at LC de Villiers sports grounds.

produce the basal plane for height estimations. This is compounded if cameras are spaced too far apart (Fig. S10). Additionally, the horizontal area behind the object of interest tapers as the fields of view from the three nearby cameras begin to wrap around the focal object, preventing a continuous area of measurable flight height. Cameras spaced closer together have a higher degree of overlap in their fields of view and the overlapping horizontal area ($m^2$) covered increases more per unit distance, encompassing a larger horizontal surface overall, improved slightly by angling the configuration. Furthermore, the point at which the three fields of view overlap is much closer to the camera configuration (Fig. S7). However, straight configurations improved the vertical coverage by not having to angle the outer cameras as much downwards relative to the central camera. Overall, the camera configurations only deviated slightly in maximising the measurable height, so long as they were not positioned too near the focal object and/or spaced too far apart.

**Discussion**

Our stereophotogrammetry approach accurately measures flight height above the ground plane for multiple bird species, approximately 35 to 275 m away from cameras. The method's application to measure bird flight height, especially near tall structures (e.g. wind-turbines) is evident. This approach overcomes some limitations and challenges posed by previous methods. Firstly, photogrammetry applies to bird species of varying size, flying speed, and turning angle. Importantly, the species-wide applicability mirrors the species-wide risk of collision (Drewitt & Langston, 2006; Marques *et al.*, 2014; Thaxter *et al.*, 2017; Perold, Ralston-Paton & Ryan, 2020). Secondly, the equipment is relatively compact and inexpensive (*ca* US$2 000 excluding costs for manual processing) compared to radar systems (*ca* US$60 000) and does not require additional cameras for confirmation of bird sightings and species. Stereophotogrammetry is preferential for small areas of interest with a few camera configurations but becomes infeasible relative to radar covering several kilometres at larger wind farms. Manual processing time costs would decrease with control points for scale, and applied object detection and machine learning models to automatically identify and track birds from the background and clutter (Betke *et al.*, 2007; Atanbori, 2017; Niemi & Tanttu, 2018). Thirdly, the method is objective, given visible vertical structures (e.g. trees, towers, etc.) in the scene to provide the software with cross-referenceable feature data, and a measurable scale in the vertical plane to improve accuracy. Importantly, such measurable features must be visible within multiple cameras' fields of view. Consequently, the approach may have a biased application to sites with these vertical structures. Its application and accuracy have yet to be tested without these structures such as in an offshore environment. Encouragingly, stereophotogrammetry is accurate to within 0.1 m compared to the use of, for example, rifle scopes and optical rangefinders (accurate within 1 m) (Stantial & Cohen, 2015; Harwood *et al.*, 2018). Regardless, accuracy to within 1 m is acceptable given the large scale of the rotor sweep and variance in bird flight heights.

*Method Evaluation*

Notwithstanding these advances, the field setup should be meticulously planned prior to data capture. Standardizing the photographic settings on each camera (ideally the same model) to ensure simultaneous shutter release is vital to effectively freeze birds in space and time. Given the synchronicity, high shutter speeds (1/1600s), and a known dimension present in the overlapping fields of view, the approach could be used on moving platforms for offshore sites. Offshore applications require testing.

No single camera configuration performed best. For a field of interest approximately 35 to 275 m long, a configuration with outer cameras angled approximately 10 m forward and 20 m apart from the central camera was suitable, but measurement error increases exponentially thereafter. There is an inherent bias to measure more low flights along the length of the field of view than high flights, which only enter the field of view with distance from the camera. Future studies should allow for sufficient sampling to record the full distribution of flight heights by various species or taxonomic groupings. Modifications of rarefaction sampling curves should be used to ensure sufficient representation of the stratified avian communities' use of layers of aerospace for a given area (de Vries & Walla, 1999; Marques, Pereira & Palmeirim, 2016).

Triangulating the positions of interest (e.g. bird) requires high overlap in camera fields of view and low angles of intersection (< 30°) to allow feature matching across photos (see Smartmatch® help files). Thus, small camera intersection angles (~ 5 to 25°) to the object of interest are preferable but are dictated by the distance to the object of interest and between cameras. We recommend maintaining an intersection angle of around 5° by adjusting the distance and angle between cameras, (however long that may be) to improve measurement accuracy. The trade-off between attaining area and maximum measurable heights should be noted. Area coverage is expected to increase with closely positioned cameras at greater than 50 m from a focal structure of interest. Cameras should, however, not be positioned too close to each other to maintain an angle of intersection around 5°.

The reduced accuracy in setup 1A may be attributed to the scale being set at the distance between the centre of two lenses. Although situationally useful, one needs to consider the difficulty in consistently measuring this dimension. Ideally, the scale should be set on a physical object in the field of view (e.g. pole for scaling; identifiable marks on a turbine or solar tower). Scale extrapolation measurement error can occur as the distance between the scale and object of interest (bird) increases, and the scale measure should ideally occur within the field of interest. Furthermore, the approach is limited to scenes with reference points in the vertical plane, probably preventing its application to estimate flight heights above large open planes without vertical reference points. However, enough flying birds photographed together might provide sufficient vertical reference data to create the 3-D scene.

Compared to the most accessible field approach to measuring flight height, photogrammetry generally outperforms laser-based range-finding (Desholm *et al.*, 2006; Harwood *et al.*, 2018), especially close-by (< 275 m), where image-pixels represent smaller actual distances. High-resolution camera sensors can improve this but increases the cost. Another improvement over the rangefinder is a fixed field of view that does away with human intervention to point at a flying animal of interest. Thus, one may use a programmable camera for motion detection to automatically trigger the other cameras without being present (Jampens *et al.*, 2016). Rangefinders are difficult to use for small, fast-moving birds, and likely create inherent biases for close, consistently moving, and larger birds (Desholm *et al.*, 2006; Harwood *et al.*, 2018). Unlike rangefinders, photogrammetry is useful to estimate flight heights from fast-moving birds travelling short distances (Desholm *et al.*, 2006; Stantial & Cohen, 2015) as they are essentially frozen within space and time by synchronized cameras. Furthermore, flight height data are inherently stored in sets of images, which can be returned to for remeasuring or species identification/verification. Despite the configuration of cameras and photogrammetry software costing more than a single rangefinder, we recommend photogrammetry as a more accurate, repeatable alternative. Some savings may be made by using other photo modelling software applications than PhotoModeler® products (e.g. Regard3D - free and iWitnessPro – US$2 495) with different user applications (close range, aerial, or both). We recommend further comparison with other approaches such as radar which, despite their expense and complexity, are accurate and able to cover a large area (Krijgsveld *et al.*, 2009; Strumpf *et al.*, 2011).

*Bird Flight Height*

Given the accuracy of stereophotogrammetric measures of fixed structures, we demonstrate how synchronous shutter release allows measures of birds in mid-air. However, additional sampling is needed to obtain meaningful flight height estimates. Like other studies, bird flight heights were weighted towards lower heights (Osborn & Dieter, 2009; Cook *et al.*, 2012). More comprehensive studies using this approach could derive more solid conclusions about flight heights.

The potential site-dependence of flight height is noteworthy. Most flight heights in this study were attained around a water body, possibly decreasing flight heights as aerial insectivores forage around the body of water (Corman & Garthe, 2014) or waterbirds land from foraging or roosting sites. Many sacred ibis flight heights were attained from commuting birds. Expanding sample sizes in future studies over seasons at various sites with different vegetation, topography, and surrounding structures will increase the taxonomic and ecological resolution of bird flight height data. Similar comparisons could be done for utility-scale solar-energy (USSE) towers, which show similar heights to wind turbines. However, it is difficult to identify birds contrasted against brightly lit receivers, visually or from the photos (Diehl *et al.*, 2016).

Species' flight behaviour and height are important to understand the impact of energy infrastructure on avian communities (Strumpf *et al.*, 2011). We need an effective approach that not only measures bird flight height but also behavioural changes when presented with tall structures such as turbines (de Lucas *et al.*, 2008; Furness, Wade & Masden, 2013). Our photogrammetric approach can address this demand by taking successive sets of images (supplementary S1). Fox *et al.* (2006) note that knowledge of 3-D flight patterns is necessary to prevent the siting of wind farms in high-risk collision areas. Photogrammetry of bird flight tracks after construction may improve our understanding of avoidance and/or attraction behaviour. Future studies need to consider the skewed impact on insectivorous birds, which are attracted by photophilic insects to illuminated receivers of USSE towers (Diehl *et al.*, 2016) or turbine collision by central place foraging raptors nesting nearby (Eichhorn *et al.*, 2012). Regardless of behaviour, flight height data may be aggregated to produce high-resolution 3-D frequency distributions of bird flight heights (Péron *et al.*, 2017, 2020). Models that use such frequency distributions to predict collision probability are reliant on accurate flight height measurements (Péron *et al.*, 2017, 2020).

Species identification was done post-hoc from the photographs. However, a large proportion of birds measured in the study were unidentified. Species identification can be improved by recording species in the field and cross-referencing identities with photos, or taking higher-resolution photographs to identify more distant birds post-hoc; possibly reducing the distance error associated with image pixilation. Using this approach, we foresee a trade-off between camera expenditure and error with increasing distance associated with image pixilation. We recommend prioritizing the former where expense is not an issue. Furthermore, species identification, from the same images used to calculate height and behavioural covariates, such as flapping rate, flight patterns, or velocity, may be automated through machine learning (Atanbori, 2017; Niemi & Tanttu, 2018). Photographs are already used alongside radar for species recognition of birds in flight (Niemi & Tanttu, 2018) and this stereophotogrammetry approach can ultimately remove the “middle man”.

## Conclusions

We illustrate the potential application of photogrammetrically measuring bird flight heights, which requires extended sampling and comparison against other approaches such as radar in further studies to provide added interpretations. Accurate bird flight height data could be used to inform engineers about solar/turbine/pylon design (e.g. size/height, visibility, number, and layout), prior to construction to minimise collision risk. The method is also applicable to existing infrastructure, where flight patterns can be assessed to identify species flight behaviour, vulnerability, mortality risk, and implement management protocols to minimise the environmental impact of pylons, solar farms and wind turbines.


## Acknowledgements

We thank the Tshwane Technology Innovation Agency (TIA) for funding. The project was initiated as part of a project assessing the impacts of industrial-scale solar power generation, supported by a grant from the Hans Hoheisen Charitable Trust. Francis Martens of Nelson Mandela University assisted with some fieldwork.


## Author contributions

de Bruyn PJN and Ryan PG conceived, designed, and revised the project. Prinsloo N, Postma M, and Coetzee M contributed to data acquisition, analysis, interpretation, drafting, and revision of the article.

## Work cited


Atanbori, J. (2017). *Automatic classification of flying bird species using computer vision techniques* (Doctor of Philosophy). Lincoln: University of Lincoln.

Baerwald, E. F., Genevieve, H., & Barclay, R. M. R. (2008). Barotrauma is a significant cause of bat fatalities at wind turbines. *Curr. Biol.*, *18*, 695–696.

Band, B. (2012). *Using a collision risk model to assess bird collision risks for offshore windfarms*. St Andrews: British Trust for Ornithology.

Barrios, L., & Rodriguez, A. (2004). Behavioural and environmental correlates of soaring-bird mortality at on-shore wind turbines. *J. Appl. Ecol.*, 41, 72–81.

Betke, M., Hirsh, D. E., Bagchi, A., Hristov, N. I., Makris, N. C., & Kunz, T. H. (2007) Tracking large variable numbers of objects in clutter. In *Computer Vision and Pattern Recognition, 2007. CVPR'07*. IEEE Conference on, IEEE, 1–8.

Blender Online Community (2019). *Blender – a 3D modelling and rendering package (version 2.80)*. Amsterdam: Blender Institute. Available at: https://www.blender.org/ (Accessed 1 August 2019).

Borkenhagen, K., Corman, A.M., & Garthe, S. (2018). Estimating flight heights of seabirds using optical rangefinders and GPS data loggers: a methodological comparison. *Mar. Biol.*, 165, 17.

Cleasby, I. R., Wakefield, E. D., Bearhop, S., Bodey, T. W., Votier, S. C., & Hamer, K. C. (2015). Three-dimensional tracking of a wide-ranging marine predator: Flight heights and vulnerability to offshore wind farms. *J. Appl. Ecol.*, *52*, 1474–1482.

Cook, A. S. C. P., Johnston, A., Wright, L. J., & Burton, N. H. K. (2012). *A review of flight heights and avoidance rates of birds in relation to offshore wind farms*. Norfolk: British Trust for Ornithology.

Corman, A.-M., & Garthe, S. (2014). What flight heights tell us about foraging and potential conflicts with wind farms: A case study in lesser black-backed gulls (*Larus fuscus*). *J. Ornithol.*, *155*, 1037–1043.

de Bruyn, P. J. N., Bester, M. N., Carlini, A. R., & Oosthuizen, W. C. (2009). How to weigh an elephant seal with one finger: A simple three-dimensional photogrammetric application. *Aquat. Biol.*, *5*, 31–39.

de Lucas, M., Guyonne, F., Janss, E., & Ferrer, M. (2008). Collision fatality of raptors in wind farms does not depend on raptor abundance. *J. Appl. Ecol.*, *45*, 1695–1703.

de Vries, P.J., & Walla, T.R. (1999). Species diversity in spatial and temporal dimensions of fruit-feeding butterflies from two Ecuadorian rainforests. *Biol. J. Linn. Soc.* 68, 333–353.

Desholm, M., Fox, A. D., Beasley, P. D. L., & Kahlert, J. (2006). Remote techniques for counting and estimating the number of bird – wind turbine collisions at sea: A review. *Ibis*, *148*, 76–89.

Diehl, R. H., Valdez, E. W., Preston, T. M., Wellik, M. J., Cryan, P. M. (2016). Evaluating the effectiveness of wildlife detection and observation technologies at a solar power tower facility. *PLoS ONE*, *11*, e0158115.

Drewitt, A. L., & Langston, R. H. W. (2006). Assessing the impacts of wind farms on birds. *Ibis*, *148*, 29–42.

Eichhorn, M., Johst, K., Seppelt, R., & Drechsler, M. (2012). Model-Based Estimation of Collision Risks of Predatory Birds with Wind. *Ecol. Soc*. 17, 1.

Everaert, J. (2014). Collision risk and micro-avoidance rates of birds with wind turbines in Flanders. *Bird Study*, 61, 220–230.

Everaert, J., & Stienen, E.W. (2006). Impact of wind turbines on birds in Zeebrugge (Belgium). In *Biodiversity and Conservation in Europe*: 103-117. Hawksword, D. L., & Bull, A. T. (Ed.). Dordrecht: Springer.

Ferrer, M., de Lucas, M., Janss, G.F., Casado, E., Munoz, A.R., Bechard, M.J., & Calabuig, C.P. (2012). Weak relationship between risk assessment studies and recorded mortality in wind farms. *J. Appl. Ecol.*, 49, 38–46.

Fox, A. D., Desholm, M., Kahlert, J., & Christensen, T. K. (2006). Information needs to support environmental impact assessment of the effects of European marine offshore wind farms on birds. *Ibis*, *148*, 129–144.

Furness, R. W., Wade, H. M., & Masden, E. A. (2013). Assessing vulnerability of marine bird populations to offshore wind farms. *J. Environ. Manage.*, *119*, 56–66.

Garthe, S., Guse, N., Montevecchi, W. A., Rail, J., & Grégoire, F. (2014). The daily catch: Flight altitude and diving behavior of northern gannets feeding on Atlantic mackerel. *J. Sea Res.*, *85*, 456–462.

Gauthreaux, S. A., & Livingston, J. W. (2006). Monitoring bird migration with a fixed-beam radar and a thermal-imaging camera. *J. Field Ornithol.*, *77*, 319–328.

Harwood, A.J., Perrow, M.R., & Berridge, R.J. (2018). Use of an optical rangefinder to assess the reliability of seabird flight heights from boat-based surveyors: implications for collision risk at offshore wind farms. *J. Field Ornithol.*, 89, 372–383.

Hill, D., & Arnold, R. (2012). Building the evidence base for ecological impact assessment and mitigation. *J. Appl. Ecol.*, *49*, 6–9.

Jampens, R. T., Hernandez, F., Vandecasteele, F., & Verstockt, S. (2016). Automatic detection, tracking and counting of birds in marine video content. In *2016 Sixth International Conference on Image Processing Theory, Tools and Applications (IPTA)* (p. 7821031). IEEE.

Jeal, C., Perold, V., Ralston-paton, S., & Ryan, P.G. (2019a). Impacts of a concentrated solar power trough facility on birds and other wildlife in South Africa. *J. African Ornithol.*, 90, 129–137.

Jeal, C., Perold, V., Seymour, C.L., Ralston-paton, S., & Ryan, P.G. (2019b). Utility-scale solar energy facilities – Effects on invertebrates in an arid environment. *J. Arid Environ.*, 168, 1–8.

Khan, J., & Arsalan, M. H. (2016). Solar power technologies for sustainable electricity generation – A review. *Renew. Sust.*, *55*, 414–425.

Krijgsveld, K.L., Akershoek, K., Schenk, F., Dijk, F., & Dirksen, S. (2009). Collision risk of birds with modern large wind turbines. *Ardea,* 97, 357–366.

Leung, D. Y. C., & Yang, Y. (2012). Wind energy development and its environmental impact: A review. *Renew. Sust.*, *16*, 1031–1039.

Marques, A. T., Batalha, H., Rodrigues, S., Costa, H., Pereira, M. J. R., Fonseca, C., Mascarenhas, M., & Bernardino, J. (2014). Understanding bird collisions at wind farms: An updated review on the causes and possible mitigation strategies. *Biol. Conserv.*, *179*, 40–52.

Marques, J.T., Pereira, M.J.R., & Palmeirim, J.M. (2016). Patterns in the use of rainforest vertical space by Neotropical aerial insectivorous bats: all the action is up in the canopy. *Ecography*, 39, 476–486.

Masden, E. A., Fox, A. D., Furness, R. W., Bullman, R., & Haydon, D. T. (2010). Cumulative impact assessments and bird / wind farm interactions: Developing a conceptual framework. *Environ. Impact Assess. Rev.*, *30*, 1–7.

Niemi, J., & Tanttu, J. T. (2018). Deep learning case study for automatic bird identification. *Appl. Sci., 8*, 2089.

Osborn, R. G., & Dieter, C. D. (2009). Bird flight characteristics near wind turbines in Minnesota. *Am. Midl. Nat.*, *139*, 29–38.

Peña, E., & Slate, E. (2006). Global validation of linear models assumptions (gvlma). *J. Am. Stat. Assoc.*, *101*, 341–354.

Perold, V., Ralston-Paton, S., & Ryan, P. (2020). On a collision course? The large diversity of birds killed by wind turbines in South Africa. *Ostrich*, 91, 228–239.

Péron, G., Calabrese, J.M., Duriez, O., Fleming, C.H., García-Jiménez, R., Johnston, A., Lambertucci, S.A., Safi, K., & Shepard, E.L. (2020). The challenges of estimating the distribution of flight heights from telemetry or altimetry data. *Anim. Biotelemetry*, 8, 1–13.

Péron, G., Fleming, C.H., Duriez, O., Fluhr, J., Itty, C., Lambertucci, S., Safi, K., Shepard, E.L., & Calabrese, J.M. (2017). The energy landscape predicts flight height and wind turbine collision hazard in three species of large soaring raptor. *J. Appl. Ecol.*, 54, 1895–1906.

Poliigon – An online assets library for the 3D community. QLD: Australia. CG Fort LTD.

Postma, M., Bester, M. N., & de Bruyn, P. J. N. (2013). Age-related reproductive variation in a wild marine mammal population. *Polar Biol.*, *36*, 719–729.

R Core Team, R. (2018). R: A language and environment for statistical computing. Vienna: R Foundation for Statistical Computing.

Saidur, R., Rahim, N. A., Islam, M. R., & Solangi, K. H. (2011). Environmental impact of wind energy. *Renew. Sust.*, *15*, 2423–2430.

Stantial, M. L., & Cohen, J. B. (2015). Estimating flight height and flight speed of breeding piping plovers, *J. Field Ornithol.*, *86*, 369–377.

Stewart, G. B., Pullin, A. S., & Coles, C. F. (2007). Poor evidence-base for assessment of windfarm impacts on birds. *Environ. Conserv.*, *34*, 1–11.

Strumpf, J.P., Denis, N., Hamer, T.E., Johnson, G., & Verschuyl, J. (2011). Flight height distribution and collision risk of the marbled murrelet *Brachyramphus marmoratus*: methodology and preliminary results. *Mar. Ornithol.*, 128, 123–128.

Thaxter, C.B., Buchanan, G.M., Carr, J., Butchart, S.H., Newbold, T., Green, R.E., Tobias, J.A., Foden, W.B., O'Brien, S., & Pearce-Higgins, J.W. (2017). Bird and bat species' global vulnerability to collision mortality at wind farms revealed through a trait-based assessment. *Proceedings of the Royal Society B: Biological Sciences*, 284, 20170829.

Theriault, D., Wu, Z., Hristov, N., Swartz, S., Breuer, K., Kunz, T., & M. Betke. (2010). *Reconstruction and analysis of 3d trajectories of Brazilian free-tailed bats in flight.* CS Department, Boston University.

Visser, E., Perold, V., Ralston-paton, S., Cardenal, A.C., & Ryan, P.G. (2019). Assessing the impacts of a utility-scale photovoltaic solar energy facility on birds in the Northern Cape, South Africa. *Renew. Energy*, 133, 1285–1294.

Walston, L. J., Rollins, K. E., LaGory, K. E., Smith, K. P., & Meyers, S. A. (2016). A preliminary assessment of avian mortality at utility-scale solar energy facilities in the United States. *Renew. Energy, 92*, 405–414.

Wand, M. (2013). KernSmooth: Functions for kernel smoothing for Wand & Jones (1995). R package version 2.23-10. http://CRAN.R-project.org/package=KernSmooth.

Wickham, H. (2016). ggplot2: Elegant Graphics for Data Analysis. New York: Springer-Verlag.

Wu, T., Hristov, N., Kunz, T., & Betke, M. (2009). Tracking-reconstruction or reconstruction-tracking? Comparison of two multiple hypothesis tracking approaches to interpret 3D object motion from several camera views. In *Workshop on Motion and Video Computing (WMVC)*. CS Department, Boston University.

Wulff, S. J., Butler, M. J., & Ballard, W. B. (2016). Assessment of diurnal wind turbine collision risk for grassland birds on the Southern Great Plains. *J. Fish Wildl. Manag., 7*, 129–140.